ARTICLE INFO

Article ID: 15-16-02-0007
© 2023 Volvo Car Corporation
doi:10.4271/15-16-02-0007

Linear and Nonlinear Kinematic Design of Multilink Suspension

Yansong Huang,[1,2] Tobias Brandin,[2] and Bengt Jacobson[1]

[1]Chalmers University of Technology, Vehicle Engineering and Autonomous Systems, Sweden
[2]Volvo Car Corporation, Sweden

Abstract

In the design of suspensions for passenger cars, it is time-consuming to find a solution that works for both kinematics and packaging. The design must provide clash-free packaging within the suspension components and sufficient clearance to surrounding parts, such as the body and the subframe. In addition, the design has to ensure a reasonable kinematic performance, in which the dynamic behaviors of the car are safe and stable at all speeds. The objective of this study was to provide a method that automatically controls specified linear and nonlinear kinematic targets at the same time as engineers test different packaging solutions. The kinematic performance is controlled when design engineers test different packaging solutions by using the proposed method. The method optimizes the linearized constraint matrices by means of given performance targets as input and proposes a hardpoint configuration. The result shows a major potential to reduce design lead time by using this method. We conclude that the design of the suspension architecture can be more efficient and precise by automatic kinematic control.

History

Received: 07 Jul 2022
Revised: 24 Aug 2022
Accepted: 15 Nov 2022
e-Available: 08 Dec 2022

Keywords

Passenger car, Kinematics, Packaging, Wheel suspension, Target, Hardpoint

Citation

Huang, Y., Brandin, T., and Jacobson, B., “Linear and Nonlinear Kinematic Design of Multilink Suspension,” *SAE Int. J. Passeng. Veh. Syst.* 16(2):105–117, 2023, doi:10.4271/15-16-02-0007.

ISSN: 2770-3460
e-ISSN: 2770-3479

© 2023 Volvo Car Corporation. Published by SAE International. This Open Access article is published under the terms of the Creative Commons Attribution Non-Commercial License (http://creativecommons.org/licenses/by-nc/4.0), which permits noncommercial use, distribution, and reproduction in any medium, provided that the original author(s) and the source are credited.

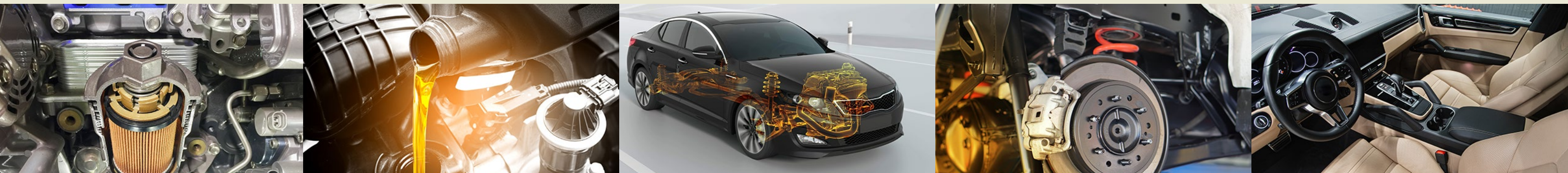

1. Introduction

Suspension systems have great impact on the complete behavior of a vehicle. The suspension plays a skeleton role of the whole car and influences many complete vehicle attributes. These attributes are usually the key to identifying vehicle characteristics. For example, a comfort-oriented car will have different attribute settings than a sports-oriented car. To achieve certain attributes such as understeer behaviors while cornering, suspension kinematics usually has a very large impact. Thus, the kinematic behaviors of passenger car suspension have been extensively studied. One of the crucial concerns is computing the kinematic behaviors.

There are two methods for precise computing of the kinematics. The first method was investigated to analyze the kinematics from hardpoints by formulating velocity constraints [1]. The method transfers certain hardpoint configurations to general motions. Then the kinematics of the suspension are expressed from general motions. Albers [2] has further investigated a larger scope of kinematic behaviors from general motions into kinematic targets including suspension steering and jounce maneuvers. The second method is an analytical approach using Jacobian differentiation. This approach developed by Hazem [3] includes the possibility to formulate a constraints matrix by differentiation. It provides a straight approach to derive the acceleration constraints by differentiating the position constraints twice. The second method is more computationally heavy but requires less modeling work compared with the first method. There are several ways to utilize the kinematic calculations. Visualization is an important method to interpreting kinematic performance through visualization of geometry features such as steering kingpin axle and roll center [4, 5]. Sommer III [6] shows a calculation method to visualize the features of first- and second-order instant screw. These geometry features can be derived from kinematic targets and guide suspension design engineers to design hardpoints.

The task of suspension design engineers is essentially to reverse the above procedures, which means that the reverse algorithms should provide hardpoints with specific kinematic targets as input. It would therefore be interesting to investigate a method, which partly controls the hardpoints according to targets. A method of this type has been developed by Huang [7]. The method provides certain hardpoint design guidelines with specific first-order linear targets. The model allows for the introduction of more targets and hence of reducing the design degree of freedom even further. This article will investigate new hardpoints control methods from the first-order linear targets and introduce additional hardpoints control method from the high order targets. In order to reverse the traditional design process, attribute leaders need to provide targets before applying this algorithm, and the method will calculate hardpoints and leave the auxiliary design control points for packaging engineers. This method shows great time-saving potentials for both packaging engineers and attribute leaders since the trial-and-error work for both sides are significantly reduced. Furthermore, this method also allows for a quick copying of many complete kinematic curves, while adjusting individual packaging constraints and targets. The engineering efficiency potential is astonishing as the design engineers, typically, can save more than half of the developing time.

1.1. Suspension System and Coordinates

The method considers steering and jounce motion targets. Therefore, a multilink rear axle with steering feature is used as example for this study. Figure A.1 shows a typical five link rear suspension layout and its nomenclature. A three-dimensional reference system according to ISO 4130:1978[1] has been selected as coordinate system.

1.2. Targets Selection

The targets that indicate suspension performance are set by the attribute leaders. It is the result of how the attribute leaders break down the requirements from complete vehicle motions to several subsystems, such as front axle and rear axle. The targets are sometimes called key performance indicators (KPI). The KPIs can be measured from physical test rigs or virtual simulations. Most of the kinematic targets are influenced by the hardpoints setup. The pre-selected kinematic targets will be transferred to hardpoints layout with the help of the presented method later on. Table 1 shows the selected targets including first, second and third order for jounce

[1] https://www.iso.org/standard/9886.html

TABLE 1 Selected targets indicating rear suspension performance.

	Jounce			Steering
Order	First order	Second order	Third order	First order
	1st Bump steer	2nd Bump steer	3rd Bump steer	Hub trail
	1st Bump camber	2nd Bump camber	3rd Bump camber	Scrub radius
	1st (Kinematic) Anti-squat	2nd Anti-squat	3rd Anti-squat	Kingpin offset
	1st (Kinematic) Anti-lift	2nd Anti-lift	3rd Anti-lift	Caster trail
	1st Roll center height (RCH)	2nd RCH	3rd RCH	Wheel load lever arm (WLLA)

© Volvo Car Corporation

Note: This is an introduction of selected kinematic targets. More detailed definitions will be introduced in the section 3.

motion and first order for steering motion. These targets are defined at the design height for the left corner model.

2. Modeling of the Multilink Axle

The modeling part consists of velocity, acceleration, and jerk analyses. Jerk as the time derivative of acceleration was studied by Ioana [8]. The velocity and angular velocity at wheel center will be calculated using velocity constraints. Then Jacobian methods will be used to derive the acceleration as well as the jerk motions.

2.1. Velocity Constraints

The velocity analysis needs to solve the general motion $\boldsymbol{V_o}$, $\boldsymbol{\omega_o}$ at wheel center for jounce and steer motions. A simple model to calculate jounce motion for multilink is demonstrated. Equation 2.1 shows the velocity constraint for each individual link with the reference from Figure A.1.

$$\left(\mathbf{V}_o + \omega_o \times \mathbf{L}_{i'o}\right) \cdot \mathbf{L}_{i'i} = 0 \qquad \text{Eq. (2.1)}$$

where

$i = A, B, C, D, E$

$\mathbf{L}_{i'i} = d(i, i')$, d is the euclidean distance

$\mathbf{L}_{i'o} = d(i', o)$

Equation 2.1 can be written with matrix form with generalized coordinates $\dot{\mathbf{q}} = \left[\mathbf{V}_o^T, \omega_o^T\right]^T$ and Jacobian matrix $[C_q]$. Equation 2.2 can be partitioned as Equation 2.3.

$$\left[C_q\right] \cdot \dot{\mathbf{q}} = 0 \qquad \text{Eq. (2.2)}$$

$$\left[C_u\right] \cdot \dot{\mathbf{u}} - \left[C_w\right] \cdot \dot{\mathbf{w}} = 0 \qquad \text{Eq. (2.3)}$$

where

$\dot{\mathbf{u}} = \left[V_{ox}, V_{oy}, \omega_{oy}, \omega_{oy}, \omega_{oz}\right]$

$\dot{\mathbf{w}} = V_{oz}$

$[C_u]$ shows in Equation B.1

$[C_w]$ shows in Equation B.2

With V_{oz} given, $\dot{\mathbf{u}}$ can be calculated and the general velocities at wheel center point O are then known. The velocities of any hardpoints at knuckle can be calculated from Equation 2.4

$$\mathbf{V}_i' = \mathbf{V}_o + \omega_o \times \mathbf{L}_{i'o} \qquad \text{Eq. (2.4)}$$

where $i = A, B, C, D, E$.

The velocity constraints for steering motion should be derived with the same principle as Equation 2.1. $\mathbf{L}_{F'F}$ should keep length fixed while applying steering motion from toelink $\mathbf{L}_{C'C}$. However, the mechanism of $\mathbf{L}_{D'D}$, $\mathbf{L}_{F'F}$ needs to be modeled with additional generalized coordinates. The steering feature will not be further included in the example of the present article.

2.2. Acceleration Constraints

The acceleration constraints in Equation 2.5 can be derived from differentiation of Equation 2.2.

$$\left[C_q\right]\ddot{\mathbf{q}} + \left[\dot{C}_q\right]\dot{\mathbf{q}} = 0 \qquad \text{Eq. (2.5)}$$

where $\left[\dot{C}_q\right]$ shows in Equation B.3.

Similarly, Equation 2.5 can be partitioned as Equation 2.6.

$$\left[C_u\right]\ddot{\mathbf{u}} - \left[C_w\right]\ddot{\mathbf{w}} + \left[\dot{C}_q\right]\dot{\mathbf{q}} = 0 \qquad \text{Eq. (2.6)}$$

where $\ddot{\mathbf{u}} = \left[a_{ox}, a_{oy}, \alpha_{ox}, \alpha_{oy}, \alpha_{oz}\right]$.

Equation B.3 shows that $\dot{C}_q$ is proportional to $\dot{\mathbf{q}}$. As a result, Equation 2.6 shows a linear relationship between $\ddot{\mathbf{u}}$ and $\dot{\mathbf{q}}^2$ if and only if $\ddot{\mathbf{w}}$ is zero. So, $\ddot{\mathbf{w}}$ is zero because V_{Oz} is given as constant. Furthermore, this assumption will simplify the derivation of the jerk motions. $\ddot{\mathbf{u}}$ can be calculated from given $\dot{\mathbf{q}}$ from Equation 2.7. Then the acceleration of any hardpoints at knuckle can be calculated from Equation 2.8.

$$\left[C_u\right]\ddot{\mathbf{u}} + \left[\dot{C}_q\right]\dot{\mathbf{q}} = 0 \qquad \text{Eq. (2.7)}$$

$$\mathbf{a}_i' = \mathbf{a}_o + \alpha_o \times \mathbf{L}_{i'o} + \omega_o \times \left(\omega_o \times \mathbf{L}_{i'o}\right) \qquad \text{Eq. (2.8)}$$

where $i = A, B, C, D, E$.

2.3. Jerk Constraints

The jerk motion $\dddot{\mathbf{u}}$ is the time derivative of acceleration. Considering derivative of Equation 2.7 with respect to time, Equation 2.9 can be formulated. Since $\dddot{\mathbf{w}}$ is assumed to be zero, $\left[C_q\right]\dddot{\mathbf{q}}$ is equal to $\left[C_u\right]\dddot{\mathbf{u}}$. Therefore, Equation 2.9 can be rewritten as Equation 2.10.

$$\left[\dot{C}_u\right]\ddot{\mathbf{u}} + \left[C_u\right]\dddot{\mathbf{u}} + \left[\ddot{C}_q\right]\dot{\mathbf{q}} + \left[\dot{C}_q\right]\ddot{\mathbf{q}} = 0 \qquad \text{Eq. (2.9)}$$

$$2 \cdot \left[\dot{C}_q\right]\ddot{\mathbf{q}} + \left[C_u\right]\dddot{\mathbf{u}} + \left[\ddot{C}_q\right]\dot{\mathbf{q}} = 0 \qquad \text{Eq. (2.10)}$$

where

$\left[\ddot{C}_q\right]$ shows in Equation B.4

$\dddot{\mathbf{u}} = \left[j_{ox}, j_{oy}, \phi_{ox}, \phi_{oy}, \phi_{oz}\right]$

As a summary, $\dot{\mathbf{u}}, \ddot{\mathbf{u}}, \dddot{\mathbf{u}}$ can be calculated with hardpoints and $\dot{\mathbf{w}}$ which is V_{oz} for the jounce motion. The general motions $\dot{\mathbf{q}}, \ddot{\mathbf{q}}, \dddot{\mathbf{q}}$ will be used to define targets in the section 3.

3. Target Identification

The general motions $\dot{\mathbf{q}}$ and their derivative $\ddot{\mathbf{u}}, \dddot{\mathbf{u}}$ are calculated from Section 2. They are the instant kinematic behaviors at design position. However, the general motions are the numerical expression, and they do not directly reflect the suspension behaviors from an engineer's point of view. Therefore, the general motions are transferred to performance targets. Table 1 shows the selected targets for both jounce and steering motions. This section defines the relation between the general motions and the targets. The first-order targets defined from Huang [7] are used to derive the second- and third-order targets.

3.1. First-Order Target

The first-order targets are defined using velocities and angular velocities. They represent the change of position measurements at wheel center and contact point. The contact point between the tire and ground is named P, and toe δ and camber γ define the wheel orientation. For steering motion, the velocities and angular velocities measured at point O are $\mathbf{V}_o^{'}, \boldsymbol{\omega}_o^{'}$. The velocity at contact point can be calculated from Equations 3.1 and 3.2. Equation 3.3–3.12 define the targets from Table 1 in detail. The definitions are recalled from Huang [7] at reference coordinate system.

$$\mathbf{V}_P = \mathbf{V}_o + \boldsymbol{\omega}_o \times \mathbf{L}_{po} \qquad \text{Eq. (3.1)}$$

$$\mathbf{V}_P^{'} = \mathbf{V}_o^{'} + \boldsymbol{\omega}_o^{'} \times \mathbf{L}_{po} \qquad \text{Eq. (3.2)}$$

$$\text{1st Bump steer} = \frac{\omega_\delta}{V_{oz}} \qquad \text{Eq. (3.3)}$$

$$\text{1st Bump camber} = \frac{\omega_{ox}\cos(\delta) - \omega_{oy}\sin(\delta)}{V_{oz}} \qquad \text{Eq. (3.4)}$$

$$(\text{Kinematic})\ \text{1st Anti-squat} = \frac{V_{ox}}{V_{oz}} \qquad \text{Eq. (3.5)}$$

$$(\text{Kinematic})\ \text{1st Anti-lift} = \frac{V_{Px}}{V_{Pz}} \qquad \text{Eq. (3.6)}$$

$$\text{1st RCH} = P_y \cdot \frac{V_{Py}}{V_{Pz}} \qquad \text{Eq. (3.7)}$$

$$\text{Hub trail} = \frac{-\left(V_{oy}^{'}\cos(\delta) + V_{ox}^{'}\sin(\delta)\right)}{\omega_\delta^{'}} \qquad \text{Eq. (3.8)}$$

$$\text{Kingpin offset} = \frac{V_{ox}^{'}\cos(\delta) - V_{oy}^{'}\sin(\delta)}{\omega_\delta^{'}} \qquad \text{Eq. (3.9)}$$

$$\text{Caster trail} = \frac{-\left(V_{px}^{'}\sin(\delta) + V_{py}^{'}\cos(\delta)\right)}{\omega_\delta^{'}} \qquad \text{Eq. (3.10)}$$

$$\text{Scrub radius} = \frac{V_{px}^{'}\cos(\delta) - V_{py}^{'}\sin(\delta)}{\omega_\delta^{'}} \qquad \text{Eq. (3.11)}$$

$$\text{Wheel load level arm (WLLA)} = \frac{V_{pz}^{'}}{\omega_\delta^{'}} \qquad \text{Eq. (3.12)}$$

where

$$\omega_\delta = -\omega_x \tan(\gamma)\sin(\delta) - \omega_y \tan(\gamma)\cos(\delta) + \omega_z$$
$$\omega_\delta^{'} = -\omega_{ox}^{'}\tan(\gamma)\sin(\delta) - \omega_{oy}^{'}\tan(\gamma)\cos(\delta) + \omega_{oz}^{'}$$

3.2. Second-Order Target

The second-order targets are defined as the time derivative of the first-order targets with respect to time. They represent the changes of the velocities. Notice that the second-order targets are always defined as targets versus V_z to make them independent of input velocity. The derivations assume a constant toe, camber angle, and the fixed contact position to simplify the expressions. The acceleration at contact point can be calculated from Equation 3.13.

$$\mathbf{a}_p = \mathbf{a}_o + \boldsymbol{\alpha}_o \times \mathbf{L}_{op} + \boldsymbol{\omega}_o \times \left(\boldsymbol{\omega}_o \times \mathbf{L}_{op}\right) \qquad \text{Eq. (3.13)}$$

$$\text{2nd Bump steer} = \frac{\frac{d}{dt}\text{Bump steer}}{V_{oz}} = \frac{\alpha_\delta}{V_{oz}^2} \qquad \text{Eq. (3.14)}$$

$$\text{2nd Bump camber} = \frac{\frac{d}{dt}\text{Bump camber}}{V_{oz}} = \frac{\alpha_{ox}\cos(\delta) - \alpha_{oy}\sin(\delta)}{V_{oz}^2} \qquad \text{Eq. (3.15)}$$

$$\text{2nd Anti-squat} = \frac{\frac{d}{dt}\text{Anti-squat}}{V_{oz}} = \frac{a_{ox}V_{oz} - a_{oz}V_{ox}}{V_{oz}^3} \qquad \text{Eq. (3.16)}$$

$$\text{2nd Anti-lift} = \frac{\frac{d}{dt}\text{Anti-lift}}{V_{oz}} = \frac{a_{px}V_{pz} - a_{pz}V_{px}}{V_{pz}^2 V_{oz}} \qquad \text{Eq. (3.17)}$$

$$\text{2nd RCH} = \frac{\frac{d}{dt}\text{RCH}}{V_{oz}} = P_y \cdot \frac{a_{py}V_{pz} - a_{pz}V_{py}}{V_{Pz}^2 V_{oz}} \qquad \text{Eq. (3.18)}$$

where

$$\alpha_\delta = -\alpha_{ox}\tan(\gamma)\sin(\delta) - \alpha_{oy}\tan(\gamma)\cos(\delta) + \alpha_{oz}.$$

3.3. Third-Order Target

Similar to the second-order targets, the third-order targets are defined as the time derivative of the second-order targets respect to time. Notice that the third-order targets always are defined as targets versus V_z^2 to making them independent of input velocity. The translational jerk at contact point can be calculated from Equation 3.19.

$$\mathbf{j}_p = \mathbf{j}_o + \phi_o \times \mathbf{L}_{op} + 2\alpha_o \times \left(\omega_o \times \mathbf{L}_{op}\right) + \omega_o \times \left(\alpha_o \times \mathbf{L}_{op}\right) + \omega_o \times \left(\omega_o \times \left(\omega_o \times \mathbf{L}_{op}\right)\right) \quad \text{Eq. (3.19)}$$

$$\text{3rd Bump steer} = \frac{\frac{dd}{dt^2}\text{Bump steer}}{V_{oz}^2} = \frac{j_\delta}{V_{oz}^3} \quad \text{Eq. (3.20)}$$

$$\text{3rd Bump camber} = \frac{\frac{dd}{dt^2}\text{Bump camber}}{V_{oz}^2} = \frac{j_{ox}\cos(\delta) - j_{oy}\sin(\delta)}{V_{oz}^3} \quad \text{Eq. (3.21)}$$

$$\text{3rd Anti-squat} = \frac{\frac{dd}{dt^2}\text{Anti-squat}}{V_{oz}^2} = \frac{j_{ox}}{V_z^3} \quad \text{Eq. (3.22)}$$

$$\text{3rd Anti-lift} = \frac{\frac{dd}{dt^2}\text{Anti-lift}}{V_{oz}^2} = \frac{\left(j_{px}V_{oz} - j_{pz}V_{ox} - a_{pz}a_{ox}\right)V_{pz}^2 - 2V_{pz}a_{pz}\left(a_{px}V_{oz} - a_{pz}V_{ox}\right)}{V_{pz}^4 V_{oz}^2} \quad \text{Eq. (3.23)}$$

$$\text{3rd RCH} = \frac{\frac{dd}{dt^2}\text{RCH}}{V_{oz}^2} = \frac{P_y}{V_{oz}^2} \cdot \frac{\left(j_{py}V_{pz} + a_{py}a_{py} - j_{pz}V_{py} - a_{pz}a_{py}\right)V_{pz}^2 - 2V_{pz}a_{pz}\left(a_{py}V_{pz} - a_{pz}V_{py}\right)}{V_{pz}^4} \quad \text{Eq. (3.24)}$$

where $j_\delta = -j_{ox}\tan(\gamma)\sin(\delta) - j_{oy}\tan(\gamma)\cos(\delta) + j_{oz}$.

In summary, the general motions $\dot{\mathbf{q}}, \ddot{\mathbf{q}}, \dddot{\mathbf{q}}$ that were calculated from Section 2 are transferred to the targets, and engineers use the targets to evaluate the kinematic performance. In the next section, a method that supports hardpoints design with targets given as input will be introduced.

4. Method to Reverse the Analysis

The method is to reverse the traditional design process. The reverse algorithm collects the performance targets as input. Then the targets are transferred to general motions and hardpoints are proposed according to general motions. The reverse method introduces control point concept and geometrical guidelines. This section describes the method step by step.

4.1. General Motions

The general motions, which include jounce motion up to third order and steering motion with first order, can be calculated from targets which are shown in Table 1 with a symbolic solver. The relations are already derived in Section 3. Figure 1 shows first-order jounce motion (blue vector) and steering motion (red vector).

4.2. Links Orientation

The design purpose is to find a setup, which gives the general motions from Figure 1 while applying jounce and steering motions. The reverse design starts with hardpoints at knuckle. Since the knuckle is a rigid body, the velocities $\hat{\mathbf{V}}_{i'j}, \hat{\mathbf{V}}_{i's}$ of any hardpoints at the knuckle can be calculated from Equation 4.1.

$$\hat{\mathbf{V}}_{i'} = \hat{\mathbf{V}}_o + \hat{\omega} \times \mathbf{L}_{i'o} \quad \text{Eq. (4.1)}$$

where $i = A, B, C, D, E$.

The links $\mathbf{L}_{A'A}, \mathbf{L}_{B'B}, \mathbf{L}_{D'D}, \mathbf{L}_{E'E}$, which control steering and jounce motions, are called support links. The link $\mathbf{L}_{C'C}$, which controls steering motion, is called toe link, and link $\mathbf{L}_{F'F}$, which controls jounce motion is called spring link. Figure 2 indicates the critical vectors to support links design. The support link, for example $B'B$, should be orthogonal to $\hat{\mathbf{V}}_{B's}$ and $\hat{\mathbf{V}}_{B'j}$. Therefore, the orientations for the support links are defined with the given point i'.

FIGURE 1 The general motions at wheel center. Solid lines with arrow head represent translational velocities $\hat{\mathbf{V}}_{oj}, \hat{\mathbf{V}}_{os}$. Dashed lines without arrow head represent angular velocities $\hat{\omega}_j, \hat{\omega}_s$.

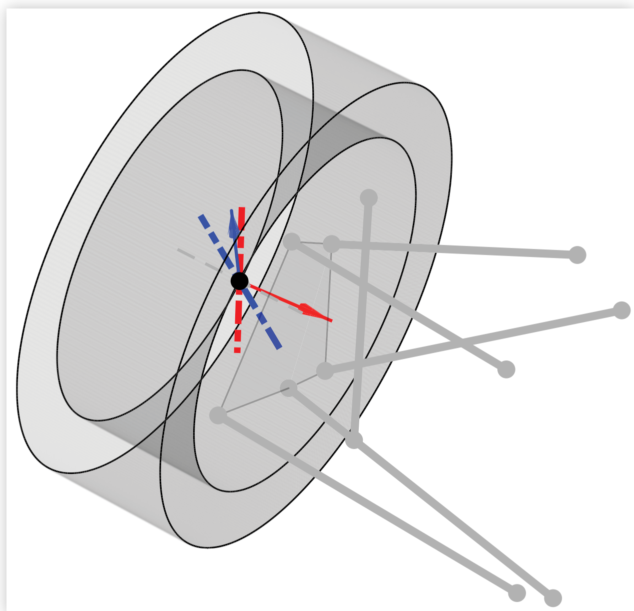

© Volvo Car Corporation

FIGURE 2 The support link, toe link, spring link design.

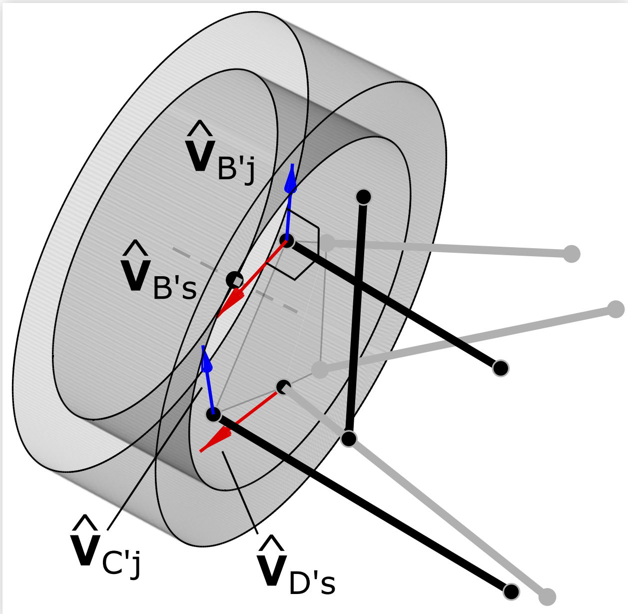

© Volvo Car Corporation

FIGURE 3 The control point **B°**.

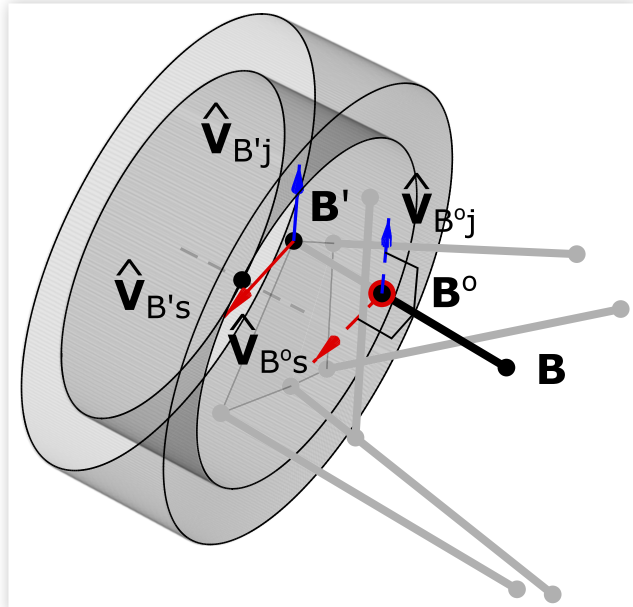

© Volvo Car Corporation

The toe link should be perpendicular to $\hat{\mathbf{V}}_{C'j}$ and the spring link should be perpendicular to $\hat{\mathbf{V}}_{C'j}$. However, their orientations are not uniquely defined. In order to uniquely determine the orientations of the toe link and spring link, additional hardpoints should be given as input. For example, hardpoints components C_{dirx}, C_{diry} and $F_y^{'}, F_y, F_z$ can be used to specify the direction of the toe link and the spring link. The hardpoint $F_y^{'}$ has great influence on the spring ratio, therefore, the position of this point should consider the kinematic performance and the packaging constraints simultaneously.

4.2.1. The Control Points

As Section 4.2 described, the orientation of the support link $L_{B'B}$ is controlled by the hardpoint $B^{'}$ and the first-order general motions. A new auxiliary point B^o located on the support link $L_{B'B}$ is introduced from Figure 3. The velocity vectors $\hat{\mathbf{V}}_{B^oj}$ and $\hat{\mathbf{V}}_{B^os}$ are rotating with respect to the support link $L_{B'B}$ from the velocity vectors $\hat{\mathbf{V}}_{B'j}$ and $\hat{\mathbf{V}}_{B's}$ because of the proportional term $\hat{\omega} \times \mathbf{L}_{i'o}$ from Equation 4.1. Therefore, the velocity vectors of any hardpoints along the support link $L_{B'B}$. are orthogonal to the support link $L_{B'B}$. In other words, the orientation of the support link $L_{B'B}$ are controlled by the auxiliary hardpoint B^o and first-order general motions, and the hardpoints $B^{'}$ and B can be any points located on the link, which was controlled by the auxiliary hardpoint B^o and first-order general motions. Thus, the auxiliary hardpoint B^o is named as the control point for link $L_{B'B}$.

In summary, the combinations of the control points and the links orientations can control the first-order targets. The hardpoint tuning possibilities have been reduced by means of predefined performance targets. The method is also called the linear control method because the method only controls the kinematic behaviors at design position. In order to precisely control the complete kinematic behaviors, the nonlinear kinematic control method is introduced in the next section.

4.3. Nonlinear Kinematic Control Method

Section 4.2 provides a method to control the first-order targets. This section introduces another approach to controlling the second- and third-order targets.

4.3.1. A Polynomial Approach

A toe curve approach with a polynomial of wheel center height (WCH) as a single indeterminate is expressed in Equation 4.2. Figure 4 shows

FIGURE 4 The polynomial nonlinear kinematic control approach.

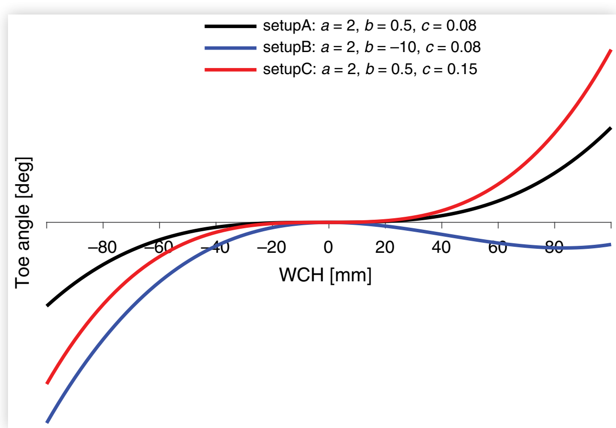

© Volvo Car Corporation

three configurations with the same first-order coefficients. The blue curve has a smaller second-order coefficient compared to the black curve, and the red curve has a larger third-order coefficient than the black curve. Figure 4 also indicates that the second-order coefficient adds a "C-shaped" curve and third-order coefficient adds a "S-shaped" curve. Therefore, the nonlinear behaviors of the toe curve can be modified by second- and third-order coefficients. The general motions of second-order $\ddot{\mathbf{q}}$ and third-order $\dddot{\mathbf{q}}$ introduced in Section 2 have similar effects, but they are applied on high dimension cases. A method using second- and third-order motions to control hardpoints will be introduced in the next section.

$$Toe = a \cdot WCH + b \cdot WCH^2 + c \cdot WCH^3 \qquad \text{Eq. (4.2)}$$

4.3.2. Link Length and Position

Section 2 shows the method to calculate $\dot{\mathbf{u}}, \ddot{\mathbf{u}}, \dddot{\mathbf{u}}$ with given $\dot{\mathbf{w}}$. Equations 4.3–4.10 show the general motions $\dddot{\mathbf{u}}$ depend on only hardpoints layout with input velocity $\dot{\mathbf{w}}$. By using the similar derivations, it can be proven that general motions $\dot{\mathbf{u}}, \ddot{\mathbf{u}}$ depend on only hardpoints layout with input velocity $\dot{\mathbf{w}}$ as well.

$$\dddot{\mathbf{u}} = \frac{1}{[C_u]}\left[-2\left[\dot{C}_u\right]\ddot{\mathbf{u}} - \left[\ddot{C}_q\right]\dot{\mathbf{q}}\right] \qquad \text{Eq. (4.3)}$$

$$= \frac{1}{[C_u]}\left[-2\left[\dot{C}_u\right]\frac{-\left[\dot{C}_q\right]\dot{\mathbf{q}}}{[C_u]} - \left[\ddot{C}_q\right]\ddot{\mathbf{q}}\right] \qquad \text{Eq. (4.4)}$$

$$= \frac{1}{[C_u]}\left[-2[K_1]\dot{\mathbf{q}}\frac{-[K_2]\dot{\mathbf{q}}\dot{\mathbf{q}}}{[C_u]} - [K_3]\ddot{\mathbf{q}}\dot{\mathbf{q}}\right] \qquad \text{Eq. (4.5)}$$

$$= \frac{1}{[C_u]}\left[-2[K_1]\dot{\mathbf{q}}\frac{-[K_2]\dot{\mathbf{q}}\dot{\mathbf{q}}}{[C_u]} - [K_3]\frac{-\left[\dot{C}_q\right]}{\left[C_q\right]}\dot{\mathbf{q}}\dot{\mathbf{q}}\right] \qquad \text{Eq. (4.6)}$$

$$= \frac{1}{[C_u]}\left[-2[K_1]\dot{\mathbf{q}}\frac{-[K_2]\dot{\mathbf{q}}\dot{\mathbf{q}}}{[C_u]} - [K_3]\frac{-[K_2]\dot{\mathbf{q}}}{\left[C_q\right]}\dot{\mathbf{q}}\dot{\mathbf{q}}\right] \qquad \text{Eq. (4.7)}$$

$$= \frac{1}{[C_u]}\left[-2[K_1]\frac{-[K_2]}{[C_u]} - [K_3]\frac{-[K_2]}{\left[C_q\right]}\right]\dot{\mathbf{q}}^3 \qquad \text{Eq. (4.8)}$$

$$= \frac{1}{[C_u]}\left[-2[K_1]\frac{-[K_2]}{[C_u]} - [K_3]\frac{-[K_2]}{\left[C_q\right]}\right]\left[\dot{\mathbf{u}}\dot{\mathbf{w}}\right]^3 \qquad \text{Eq. (4.9)}$$

$$= \frac{1}{[C_u]}\left[-2[K_1]\frac{-[K_2]}{[C_u]} - [K_3]\frac{-[K_2]}{\left[C_q\right]}\right][K_4]^3\dot{\mathbf{w}}^3 \qquad \text{Eq. (4.10)}$$

where $[K_{1,2,3,4}]$ is only depended on hardpoint according to Equations B.3 and B.4.

The dependency proof for the second-order motion $\ddot{\mathbf{u}}$ can be derived using a similar method. Since the matrices $[C_u]$, $[C_q]$, $[K_1]$, $[K_2]$, $[K_3]$, and $[K_4]$ only depend on hardpoints layout, it can be shown that $\frac{\dddot{\mathbf{u}}}{\dot{\mathbf{w}}^3}$ and $\frac{\ddot{\mathbf{u}}}{\dot{\mathbf{w}}^2}$ are constant values with given hardpoints. Since the control points and the links' orientations, which were introduced in Section 4.2, can already be used to control the first-order targets, the y coordinates of each inner point i and outer point i' can be used to control the second- and the third-order targets.

FIGURE 5 Optimize the link length and position.

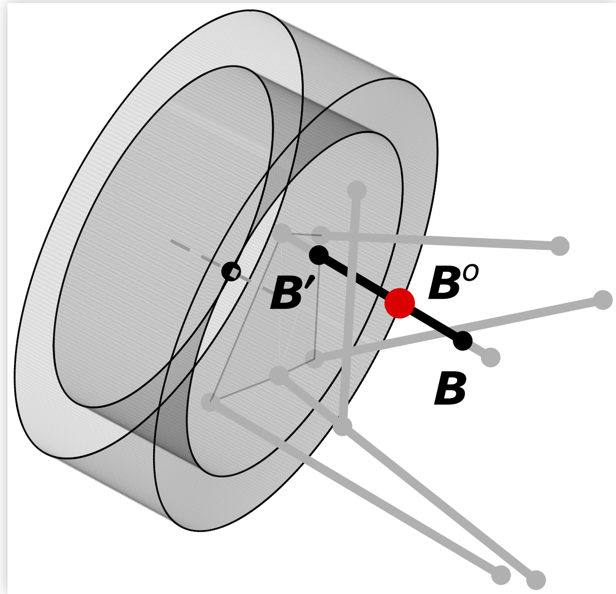

© Volvo Car Corporation

The problem can be treated as an optimization problem. The tuning parameters are the y coordinate of each inner and outer hardpoints. And the optimization goal is to find these y coordinates, which give the correct second- and third-order motions calculated from second- and third-order targets. The model in Section 2 is used to construct the optimization. Figure 5 shows the optimized hardpoints B', B with given targets and a control point B^o.

In summary, the second- and the third-order targets can be controlled by the length of the support links and their exact positions. Together with the first-order control method, all hardpoints are uniquely calculated using optimization.

4.4. Working Flow and Engineering Roles

As described in Sections 2, 4.2, and 4.3, the method can be coded with any programming language such as Python or MATLAB, and the program can run with the support from an arbitrary matrix linear algebra and nonlinear optimization packages. The program inputs are the general motions, which can be solved from the predefined targets at Table 1 by using a symbolic solver or nonlinear numerical solver. Section 3 provides mathematic expressions between the targets and the general motions. Furthermore, a pipeline can be built to provide a seamless flow.

The design process starts from defining the targets and the design geometry. Handling attribute leaders have responsibilities to define the targets, and packaging engineers need to define the design geometry. Then, the pipeline generates hardpoints automatically. If any clashes are detected, packaging engineers can change the design geometry, especially the control points mentioned in Section 4.2.1, without changing the performance targets. However, sometimes the clashes cannot be solved by just changing design geometry. Then the handling attribute leaders need to clarify some performance targets to improve the packaging situation. By using proposed workflow, one of the benefits is to separate the tasks between the handling attribute leaders and packaging engineers. Therefore, packaging engineers do not always need to wait for the handling attribute leaders to search for feasible solutions, and vice versa.

FIGURE 6 Setup with new first-order targets.

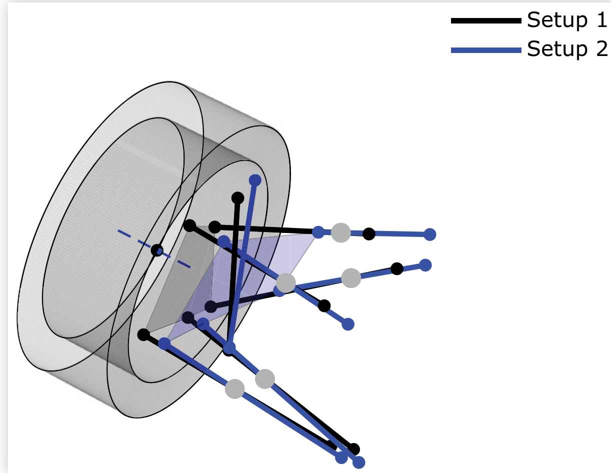

© Volvo Car Corporation

5. Application Example

A reverse design method of the multilink suspension is presented in this section. The inputs have two categories: the design geometry and the targets as mentioned in Section 4.4. The design geometry includes control points introduced from Section 4.2.1 and additional hardpoint components C_{dirx}, C_{diry}, F_y', F_y, F_z. The targets are taken from Section 1.2. The output after applying the reverse method is one unique hardpoint configuration. Four setups will be studied, and the input targets, the design geometry, and the output hardpoints are shown in Tables C.1, C.2, and D.1.

5.1. First-Order Example

The first example compares two setups that have different first-order targets. Compared with reference setup 1, setup 2 has the reduced RCH, the increased kingpin offset, and the reduced scrub radius. The design geometry is the same for all the setups. Figure 6 shows the new hardpoints layout, which is generated from the reverse algorithm. Figure E.1 shows the simulation results for different setups. Figures E.1(e), E.1(i), and E.1(l) indicate the changes of first-order targets, and the targets which are not changed from input file remain same (jounce and steering) linear and (jounce) nonlinear behaviors.

5.2. Second and Third-Order Example

The second example compares three setups, which have different second-order targets and third-order targets. Setup 3 changes the second-order bumpsteer target and setup 4 changes the third-order bumpsteer target comparing with the reference setup 1. The expected results should be similar to the polynomial behavior, which is described from Section 4.3.1. Figure 7 shows the new layouts for setups 3 and 4. The control points work as expected because all links go through the control points. Figure E.1(a) shows the change on the toe curve with added second-order C shape from setup 3 and S shape from setup 4. The results show that the shapes of the target curves can be tuned individually by introducing the second- and third-order kinematic control algorithm. As a result, the design engineers are able to change the packaging solution by changing the control points without changing the targets.

5.3. Results and Validation

Once the hardpoints are generated using the mentioned method from Section 4, the kinematic performance is evaluated by the results from simulation in Figure E.1 and the tabulated results at Table C.1. The simulation uses the methods mentioned in Sections 2 and 3. The validation is done by comparing the input targets and tabulated results, and Figure 8 shows the validation process. The algorithm successfully reverses the engineering problem when the input targets and the tabulated results become exactly the same.

FIGURE 7 Optimize the link length and position.

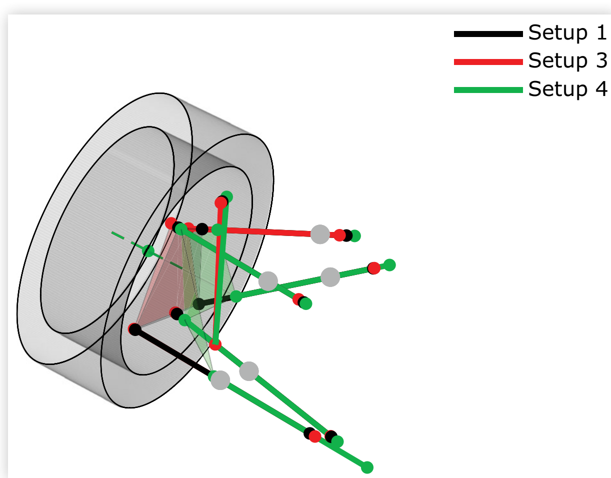

© Volvo Car Corporation

FIGURE 8 Validation process.

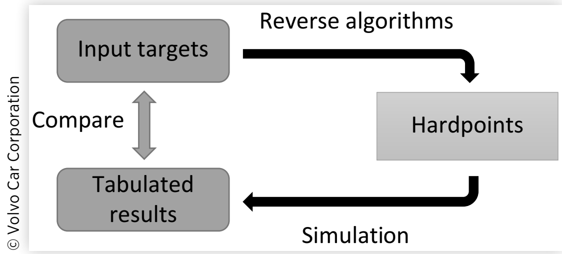

6. Conclusion

Traditional suspension design methods are based on trial-and-error is not efficient. Suspension engineers must meet packaging constraints by relying on trial-and-error iterative simulations to gradually refine the kinematic performance. Simulating suspension behaviors is also time-consuming. Therefore, a method that reduces the kinematic design lead time has been proposed. The method presented primarily addresses the kinematic design problem by reversing the traditional design procedure. The algorithm that starts from targets identification provides design guidelines, including linkage orientation, length, and position. The method includes calculations in two steps. The first step is to obtain the velocity constraints and to use first-order targets to calculate general motions. Then the hardpoints design guideline for the first-order targets control is provided from the algorithm to designers by indicating the linkage directions. The second step uses acceleration and jerk constraints, which can be obtained by partial differentiation from velocity and acceleration constraints. The exact position of the linkage can then be calculated by specifying the second-order and third-order targets.

The results show that the general motion, which includes velocity, acceleration, and jerk, is precisely controlled by this method. The result also shows that the complete design can be approached simultaneously from a feasible packaging solution and required kinematic setup, and eventually transfers into a solution that satisfies both packaging and kinematic requirements. The reverse method helps design engineers search the feasible packaging solutions more efficiently in the early design stages. Furthermore, compared with previous optimization-based methods, the new method here always provides unique solutions, which means that the targets and the hardpoints are uniquely correlated. Therefore, engineers who work with CAE and CAD parts can always build clear connections to each other by understanding the influence from both the performance and the packaging side.

Contact Information

Yansong Huang
Corresponding author
Yansong.huang@volvocars.com

Tobias Brandin
tobias.brandin@volvocars.com

Bengt Jacobson
bengt.jacobson@chalmers.se

References

1. Matschinsky, W., *Radführungen der Straßenfahrzeuge: Kinematik, Elasto-Kinematik und Konstruktion*, 3rd ed. (Berlin/Heidelberg/New York: Springer, 2007)
2. Albers, I., "Erstellung eines Berechnungstools zur starrkinematischen Analyse von Einzelradaufhängungen," Dipl.-Arb., Rheinisch-Westfälische Technische Hochschule, Aachen, 2003.
3. Attia, H.A., "Numerical Kinematic Analysis of the Standard Macpherson Motor-Vehicle Suspension System," *KSME International Journal* 17, no. 12 (2003): 1961-1968.
4. Heo, J.-H., Lee, U.-K., and Lee, S.-H., "Development of a Method to Compute the Kingpin Axis Using Screw Axis Theory Based on Suspension-Parameter Measuring Device Data," *Proceedings of the Institution of Mechanical Engineers, Part D: Journal of Automobile Engineering* 223, no. 4 (2009): 519-531, doi:10.1243/09544070JAUTO1004.
5. Lee, J.K. and Shim, J.K., "Validity and Limitations of the Kinematic Roll Center Concept from the Viewpoint of Spatial Kinematics Using Screw Theory," *International Journal of Automotive Technology* 12, no. 5 (2011): 769-775.
6. Sommer, H.J. III, "Determination of First and Second Order Instant Screw Parameters from Landmark Trajectories," *Journal of Mechanical Design* 114, no. 2 (1992): 274.
7. Yansong, H., "Knowledge and Requirements Based Wheel Suspension Template," Master thesis, Institut für Verbrennungsmotoren und Kraftfahrwesen, Universität Stuttgart, 2018.
8. Craciuna, I. and Ungureanu, M., "On Jerk in the Kinematic Study of the Rigid Body," *IOP Conference Series: Materials Science and Engineering* 749 (2020): 20.

Appendix A: Hardpoint Nomenclature

FIGURE A.1 Multilink rear suspension and nomenclature.

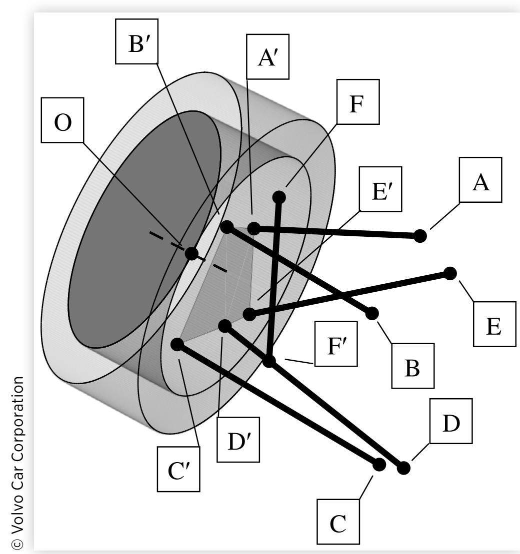

Appendix B: Constraints Matrices

$$[C_u]=\begin{bmatrix} A'x-Ax & A'y-Ay & -(A'y-Ay)(A'z-Oz)+(A'z-Az)(A'y-Oy) & -(A'y-Ay)(A'z-Oz)+(A'z-Az)(A'y-Oy) & -(A'y-Ay)(A'z-Oz)+(A'z-Az)(A'y-Oy) \\ B'x-Bx & B'y-By & -(B'y-By)(B'z-Oz)+(B'z-Bz)(B'y-Oy) & -(B'y-By)(B'z-Oz)+(B'z-Bz)(B'y-Oy) & -(B'y-By)(B'z-Oz)+(B'z-Bz)(B'y-Oy) \\ C'x-Cx & C'y-Cy & -(C'y-Cy)(C'z-Oz)+(C'z-Cz)(C'y-Oy) & -(C'y-Cy)(C'z-Oz)+(C'z-Cz)(C'y-Oy) & -(C'y-Cy)(C'z-Oz)+(C'z-Cz)(C'y-Oy) \\ D'x-Dx & D'y-Dy & -(D'y-Dy)(D'z-Oz)+(D'z-Dz)(D'y-Oy) & -(D'y-Dy)(D'z-Oz)+(D'z-Dz)(D'y-Oy) & -(D'y-Dy)(D'z-Oz)+(D'z-Dz)(D'y-Oy) \\ E'x-Ex & E'y-Ey & -(E'y-Ey)(E'z-Oz)+(E'z-Ez)(E'y-Oy) & -(E'y-Ey)(E'z-Oz)+(E'z-Ez)(E'y-Oy) & -(E'y-Ey)(E'z-Oz)+(E'z-Ez)(E'y-Oy) \end{bmatrix}$$

Eq. (B.1)

$$[C_w]=\left[A'z-Az \;\; B'z-Bz \;\; B'z-Bz \;\; -(A'y-Ay)(A'z-Oz)+(A'z-Az)(A'y-Oy) \;\; -(A'y-Ay)(A'z-Oz)+(A'z-Az)(A'y-Oy)\right]$$

Eq. (B.2)

$$[\dot{C}_q]=\begin{bmatrix} V_{A'x} & V_{A'y} & V_{A'z} & \begin{array}{c}-(A'y-Ay)(V_{A'z}-V_{Oz})-V_{A'y}(A'z-Oz)\\+(A'z-Az)(V_{A'y}-V_{Oy})+V_{A'z}(A'y-Oy)\end{array} & \begin{array}{c}(A'x-Ax)(V_{A'z}-V_{Oz})+V_{A'x}(A'z-Oz)\\-(A'z-Az)(V_{A'x}-V_{Ox})-V_{A'z}(A'x-Ox)\end{array} & \begin{array}{c}-(A'x-Ax)(V_{A'y}-V_{Oy})-V_{A'x}(A'y-Oy)\\+(A'y-Ay)(V_{A'x}+V_{Oy})-V_{A'y}(A'x-Ox)\end{array} \\ V_{B'x} & V_{B'y} & V_{B'z} & \begin{array}{c}-(B'y-By)(V_{B'z}-V_{Oz})-V_{B'y}(B'z-Oz)\\+(B'z-Bz)(V_{B'y}-V_{Oy})+V_{B'z}(B'y-Oy)\end{array} & \begin{array}{c}(B'x-Bx)(V_{B'z}-V_{Oz})+V_{B'x}(B'z-Oz)\\-(B'z-Bz)(V_{B'x}-V_{Ox})-V_{B'z}(B'x-Ox)\end{array} & \begin{array}{c}-(B'x-Bx)(V_{B'y}-V_{Oy})-V_{B'x}(B'y-Oy)\\+(B'y-By)(V_{B'x}+V_{Oy})-V_{B'y}(B'x-Ox)\end{array} \\ V_{C'x} & V_{C'y} & V_{C'z} & \begin{array}{c}-(C'y-Cy)(V_{C'z}-V_{Oz})-V_{C'y}(C'z-Oz)\\+(C'z-Cz)(V_{C'y}-V_{Oy})+V_{C'z}(C'y-Oy)\end{array} & \begin{array}{c}(C'x-Cx)(V_{C'z}-V_{Oz})+V_{C'x}(C'z-Oz)\\-(C'z-Cz)(V_{C'x}-V_{Ox})-V_{C'z}(C'x-Ox)\end{array} & \begin{array}{c}-(C'x-Cx)(V_{C'y}-V_{Oy})-V_{C'x}(C'y-Oy)\\+(C'y-Cy)(V_{C'x}+V_{Oy})-V_{C'y}(C'x-Ox)\end{array} \\ V_{D'x} & V_{D'y} & V_{D'z} & \begin{array}{c}-(D'y-Dy)(V_{D'z}-V_{Oz})-V_{D'y}(D'z-Oz)\\+(D'z-Dz)(V_{D'y}-V_{Oy})+V_{D'z}(D'y-Oy)\end{array} & \begin{array}{c}(D'x-Dx)(V_{D'z}-V_{Oz})+V_{D'x}(D'z-Oz)\\-(D'z-Dz)(V_{D'x}-V_{Ox})-V_{D'z}(D'x-Ox)\end{array} & \begin{array}{c}-(D'x-Dx)(V_{D'y}-V_{Oy})-V_{D'x}(D'y-Oy)\\+(D'y-Dy)(V_{D'x}+V_{Oy})-V_{D'y}(D'x-Ox)\end{array} \\ V_{E'x} & V_{E'y} & V_{E'z} & \begin{array}{c}-(E'y-Ey)(V_{E'z}-V_{Oz})-V_{E'y}(E'z-Oz)\\+(E'z-Ez)(V_{E'y}-V_{Oy})+V_{E'z}(E'y-Oy)\end{array} & \begin{array}{c}(E'x-Ex)(V_{E'z}-V_{Oz})+V_{E'x}(E'z-Oz)\\-(E'z-Ez)(V_{E'x}-V_{Ox})-V_{E'z}(E'x-Ox)\end{array} & \begin{array}{c}-(E'x-Ex)(V_{E'y}-V_{Oy})-V_{E'x}(E'y-Oy)\\+(E'y-Ey)(V_{E'x}+V_{Oy})-V_{E'y}(E'x-Ox)\end{array} \end{bmatrix}$$

Eq. (B.3)

$$[\ddot{C}_q]=\begin{bmatrix} a_{A'x} & a_{A'y} & a_{A'z} & \begin{array}{c}-(A'y-Ay)(a_{A'z}-a_{Oz})-a_{A'y}(A'z-Oz)\\+(A'z-Az)(a_{A'y}-a_{Oy})+a_{A'z}(A'y-Oy)\end{array} & \begin{array}{c}(A'x-Ax)(a_{A'z}-a_{Oz})+a_{A'x}(A'z-Oz)\\-(A'z-Az)(a_{A'x}-a_{Ox})-a_{A'z}(A'x-Ox)\end{array} & \begin{array}{c}-(A'x-Ax)(a_{A'y}-a_{Oy})-a_{A'x}(A'y-Oy)\\+(A'y-Ay)(a_{A'x}+a_{Oy})-a_{A'y}(A'x-Ox)\end{array} \\ a_{B'x} & a_{B'y} & a_{B'z} & \begin{array}{c}-(B'y-By)(a_{B'z}-a_{Oz})-a_{B'y}(B'z-Oz)\\+(B'z-Bz)(a_{B'y}-a_{Oy})+a_{B'z}(B'y-Oy)\end{array} & \begin{array}{c}(B'x-Bx)(a_{B'z}-a_{Oz})+a_{B'x}(B'z-Oz)\\-(B'z-Bz)(a_{B'x}-a_{Ox})-a_{B'z}(B'x-Ox)\end{array} & \begin{array}{c}-(B'x-Bx)(a_{B'y}-a_{Oy})-a_{B'x}(B'y-Oy)\\+(B'y-By)(a_{B'x}+a_{Oy})-a_{B'y}(B'x-Ox)\end{array} \\ a_{C'x} & a_{C'y} & a_{C'z} & \begin{array}{c}-(C'y-Cy)(a_{C'z}-a_{Oz})-a_{C'y}(C'z-Oz)\\+(C'z-Cz)(a_{C'y}-a_{Oy})+a_{C'z}(C'y-Oy)\end{array} & \begin{array}{c}(C'x-Cx)(a_{C'z}-a_{Oz})+a_{C'x}(C'z-Oz)\\-(C'z-Cz)(a_{C'x}-a_{Ox})-a_{C'z}(C'x-Ox)\end{array} & \begin{array}{c}-(C'x-Cx)(a_{C'y}-a_{Oy})-a_{C'x}(C'y-Oy)\\+(C'y-Cy)(a_{C'x}+a_{Oy})-a_{C'y}(C'x-Ox)\end{array} \\ a_{D'x} & a_{D'y} & a_{D'z} & \begin{array}{c}-(D'y-Dy)(a_{D'z}-a_{Oz})-a_{D'y}(D'z-Oz)\\+(D'z-Dz)(a_{D'y}-a_{Oy})+a_{D'z}(D'y-Oy)\end{array} & \begin{array}{c}(D'x-Dx)(a_{D'z}-a_{Oz})+a_{D'x}(D'z-Oz)\\-(D'z-Dz)(a_{D'x}-a_{Ox})-a_{D'z}(D'x-Ox)\end{array} & \begin{array}{c}-(D'x-Dx)(a_{D'y}-a_{Oy})-a_{D'x}(D'y-Oy)\\+(D'y-Dy)(a_{D'x}+a_{Oy})-a_{D'y}(D'x-Ox)\end{array} \\ a_{E'x} & a_{E'y} & a_{E'z} & \begin{array}{c}-(E'y-Ey)(a_{E'z}-a_{Oz})-a_{E'y}(E'z-Oz)\\+(E'z-Ez)(a_{E'y}-a_{Oy})+a_{E'z}(E'y-Oy)\end{array} & \begin{array}{c}(E'x-Ex)(a_{E'z}-a_{Oz})+a_{E'x}(E'z-Oz)\\-(E'z-Ez)(a_{E'x}-a_{Ox})-a_{E'z}(E'x-Ox)\end{array} & \begin{array}{c}-(E'x-Ex)(a_{E'y}-a_{Oy})-a_{E'x}(E'y-Oy)\\+(E'y-Ey)(a_{E'x}+a_{Oy})-a_{E'y}(E'x-Ox)\end{array} \end{bmatrix}$$

Eq. (B.4)

Appendix C: Targets and Design Geometry

TABLE C.1 Input targets which are identically same as tabulated results.

Targets	Setup 1	Setup 2	Setup 3	Setup 4
1st Bump steer [deg/m]	0.17	0.17	0.17	0.17
1st Bump camber [deg/m]	−26.17	−26.17	−26.17	−26.17
1st Anti-squat [%]	13.08	13.08	13.08	13.08
1st Anti-lift [%]	37.88	37.88	37.88	37.88
1st RCH [mm]	99.05	50	99.05	99.05
Hub trail [mm]	14.92	14.92	14.92	14.92
Kingpin offset [mm]	13.21	50	13.21	13.21
Caster trail [mm]	37.34	37.34	37.34	37.34
Scrub radius [mm]	20.24	0	20.24	20.24
WLLA [mm]	15.78	15.78	15.78	15.78
2nd Bump steer [(deg/m)/dm]	3.84	3.84	0	3.84
2nd Bump camber [(deg/m)/dm]	−12.32	−12.32	−12.32	−12.32
2nd Anti-squat [%/dm]	−13.2	−13.2	−13.2	−13.2
2nd Anti-lift [%/dm]	−8.28	−8.28	−8.28	−8.28
2nd RCH [mm/dm]	−155	−155	−155	−155
3rd Bump steer [(deg/m)/dm^2]	−6.13	−6.13	−6.13	−17.19
3rd Bump camber [(deg/m)/dm^2]	−7.96	−7.96	−7.96	−7.96
3rd Anti-squat [%/dm^2]	1.18	1.18	1.18	1.18
3rd Anti-lift [%/dm^2]	−0.43	−0.43	−0.43	−0.43
3rd RCH [mm/dm^2]	55.1	55.1	5.55.1	55.1

© Volvo Car Corporation

TABLE C.2 Design geometry.

Design geometry	Setup 1, 2, 3, 4	Design geometry	Setup 1, 2, 3, 4
O_x	0	D_x^o	90
O_y	−831.5	D_y^o	−500
O_z	0	D_z^o	−112.1
A_x^o	−190.2	E_x^o	−237
A_y^o	−500	E_y^o	−500
A_z^o	79.8	E_z^o	−95.4
B_x^o	15.5	F_y'	−605
B_y^o	−500	F_y	−542
B_z^o	108.3	F_z	414
C_x^o	199.9	—	—
C_y^o	−500	—	—
C_z^o	−40.9	—	—
C_{dirx}	214	—	—
C_{diry}	−260	—	—

The unit of hardpoint use millimeter [mm].

© Volvo Car Corporation

Appendix D: Hardpoints List

TABLE D.1 Output hardpoints.

Hardpoints	Setup 1	Setup 2	Setup 3	Setup 4
A_x	−220.98	−301.98	−212.95	−230.63
A_y	−451.00	−352.89	−463.78	−435.64
A_z	77.98	63.86	78.45	77.41
A'_x	−51.99	−162.01	−35.93	−70.02
A'_y	−720.01	−537.1	−745.57	−691.31
A'_z	87.97	83.82	88.92	86.91
B_x	18.04	21.06	17.67	18.19
B_y	−405.99	−346.98	−419.61	−400.51
B_z	99.01	82.70	100.36	98.47
B'_x	9.01	9.86	8.48	9.21
B'_y	−740.00	−655.19	−759.4	−732.41
B'_z	132.01	134.27	133.93	131.26
C_x	214	215.55	214.81	222.83
C_y	−260	−233.64	−246.28	−109.70
C_z	−47.97	−64.37	−48.37	−52.4
C'_x	186.09	189.28	185.88	198.90
C'_y	−735	−680.71	−738.66	−517.10
C'_z	−33.98	−24.98	−33.87	−40.40
D_x	143.09	152.25	142.64	146.94
D_y	−249.99	−230.95	−252.10	−231.86
D_z	−119.99	−138.94	−119.92	−120.56
D'_x	42.01	47.56	40.83	47.18
D'_y	−726.01	−683.45	−731.56	−701.65
D'_z	−104.97	−93.80	−104.79	−105.74
E_x	−298.04	−338.50	−299.50	−321.20
E_y	−424.99	−379.79	−423.21	−396.54
E_z	−76.03	−73.78	−75.57	−68.68
E'_x	−49.02	−138.86	−48.96	−102.41
E'_y	−730.99	−616.23	−731.05	−665.38
E'_z	−155.06	−116.30	−155.07	−138.11
F_x	124.27	64.73	129.31	107.81
F_y	−542.00	−542.00	−542.00	−542.00
F_z	414.00	414.00	414.00	414.00
F'_x	67.70	65.71	67.70	67.70
F'_y	−605.00	−605.00	−605.00	−605.00
F'_z	−108.79	−101.62	−108.79	−108.79

The unit of hardpoint use millimeter [mm].

© Volvo Car Corporation

Appendix E: Simulation Results

FIGURE E.1 Result from simulation.

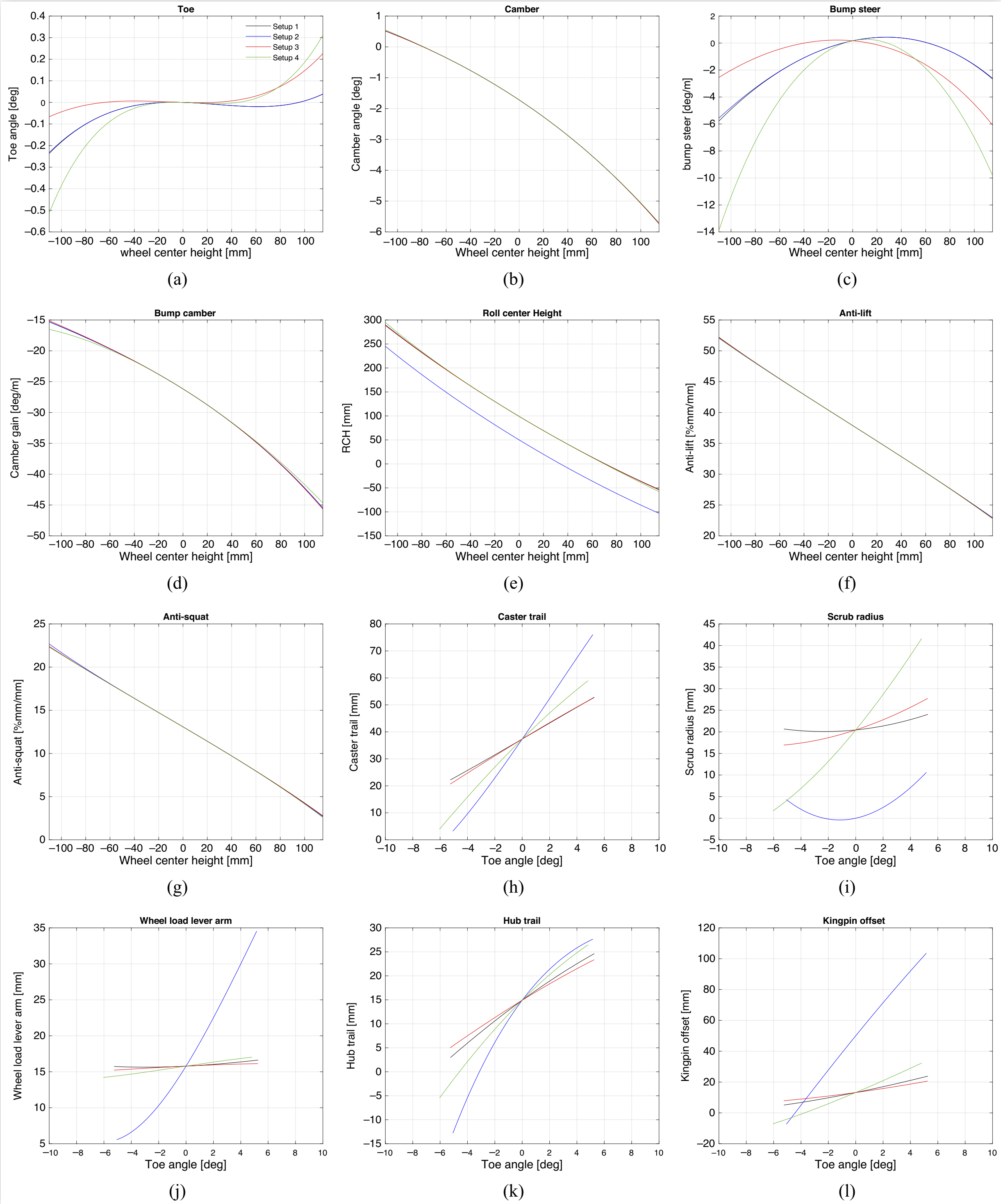

© Volvo Car Corporation

© 2023 Volvo Car Corporation. Published by SAE International. This Open Access article is published under the terms of the Creative Commons Attribution Non-Commercial License (http://creativecommons.org/licenses/by-nc/4.0), which permits noncommercial use, distribution, and reproduction in any medium, provided that the original author(s) and the source are credited.

Positions and opinions advanced in this work are those of the author(s) and not necessarily those of SAE International. Responsibility for the content of the work lies solely with the author(s).